Anisotropic magnetic properties and tunable conductivity in two-dimensional layered NaCrX$_2$ (X=Te,Se,S) single crystals

Jiale Huang, Bingxian Shi ⓘ, Feihao Pan, Jinchen Wang, Juanjuan Liu, Daye Xu, Hongxia Zhang, Tianlong Xia, and Peng Cheng ⓘ*

Laboratory for Neutron Scattering and Beijing Key Laboratory of Optoelectronic Functional Materials and MicroNano Devices, Department of Physics, Renmin University of China, Beijing 100872, China

Monolayer NaCrX$_2$ (X=Te,Se,S) was theoretically proposed to be a two-dimensional intrinsic ferromagnetic semiconductor, although its physical properties have not been thoroughly investigated in bulk single crystals. We report the single-crystal growth, structural, magnetic, and electronic transport properties of NaCr(Te$_{1-x}$Se$_x$)$_2$ ($0 \leqslant x \leqslant 1$) and NaCrS$_2$. For NaCr(Te$_{1-x}Se_x$)$_2$, the strong perpendicular magnetic anisotropy of NaCrTe$_2$ can be gradually tuned to be a nearly isotropic one by Se doping. Meanwhile, a systematic change in the conductivity with increasing x is observed, displaying a doping-induced metal-insulator-like transition. Under magnetic field larger than 30 kOe, both NaCrTe$_2$ and NaCrSe$_2$ can be polarized to a ferromagnetic state. However, for NaCrS$_2$, robust antiferromagnetism is observed up to 70 kOe, and two field-induced metamagnetic transitions are identified along $H \parallel ab$. These intriguing properties together with the potential to be exfoliated down to few-layer thickness make NaCrX$_2$ (X=Te,Se,S) promising for exploring spintronic applications.

I. INTRODUCTION

Magnetism in two dimensions has been a fascinating topic in condensed matter physics for decades. From the initial investigations on thin-film magnets to the recent discovery of two-dimensional (2D) magnetic order in ultrathin van der Waals (vdW) materials, a wide range of possibilities for both spintronic applications and fundamental research have been opened up [1–3]. For few-layer vdW crystals, 2D magnetism has been realized in metallic Fe$_3$GeTe$_2$ [4,5], semiconducting CrI$_3$/Gr$_2$Ge$_2$Te$_6$ [6,7], and insulating FePS$_3$ [8,9] due to the large magnetic anisotropy which could counteract thermal fluctuations. These materials can serve as different building blocks of vdW heterostructures depending on their conductivity and have potential applications in novel magnetoelectronic devices. Therefore, magnetic anisotropy and conductivity are two key properties of 2D magnetic materials. Finding new 2D materials and ways to tune these properties is quite important in the research on 2D magnetism.

Bulk CrTe$_2$ with a $1T$ phase is a vdW ferromagnet with in-plane magnetic anisotropy and a Curie temperature of 310 K [10]. Remarkably, in ultrathin flakes or films, the easy axis of CrTe$_2$ changes from in plane to out of plane, and room-temperature ferromagnetism is retained [11–14]. Moreover, a recent study identified a zigzag-type antiferromagnetic order in monolayer CrTe$_2$ [15], demonstrating the intricacy of 2D magnetism in this material. On the other hand, the intercalations of metal atoms into the vdW gap of CrX$_2$ (X=Te,Se,S) can form plenty of new phases. Although the structures of these intercalated CrTe$_2$ phases are

non-vdW type, many of them can still be exfoliated into nanosheets while retaining intriguing physical properties. For example, the room-temperature ferromagnetism in 10-nm-thick Cr-intercalated CrTe$_2$ [16] and the superionic behavior in 1.1-nm-thick AgCrS$_2$ [17] were reported recently. Especially for the latter, the structure of the so-called AgCrS$_2$ monolayer consists of one Ag layer sandwiched between two [CrS$_2$] layers with the actual formula AgCr$_2$S$_4$, which has been shown to be stable experimentally [17].

Na-intercalated NaCrX$_2$ (X=Te,Se,S) was recently proposed to be a class of monolayer ferromagnetic semiconductors using first-principles calculations [18]. Although the crystal structures are non-vdW type, their cleavage energies are comparable with other 2D materials. It also should be mentioned that, in previous studies the vdW magnetic material CrTe$_2$ was mainly made by deintercalating the alkali metal of KCrTe$_2$. However, the physical properties of NaCrTe$_2$ were been thoroughly investigated until recently. Experimentally, NaCrTe$_2$ was determined to be an A-type antiferromagnet with $T_N = 110$ K and perpendicular magnetic anisotropy [19,20]. With applied magnetic field, spin-flip-driven giant negative and angle-dependent magnetoresistances are observed for single crystals of NaCrTe$_2$ [20]. For NaCrSe$_2$ and NaCrS$_2$, although their antiferromagnetic transition temperature and structure have already been determined [21], the anisotropic and field-induced magnetic properties are still unclear due to the lack of single crystals. Furthermore, chemical doping has been proved to be an effective way to tune the magnetic and transport properties of layered magnetic materials [22–25]. It would be interesting to explore the Se-doping effect on NaCrTe$_2$.

In this paper, we report the successful growth of single crystals of NaCr(Te$_{1-x}$Se$_x$)$_2$ and NaCrS$_2$. These crystals

---

*Corresponding author: pcheng@ruc.edu.cn
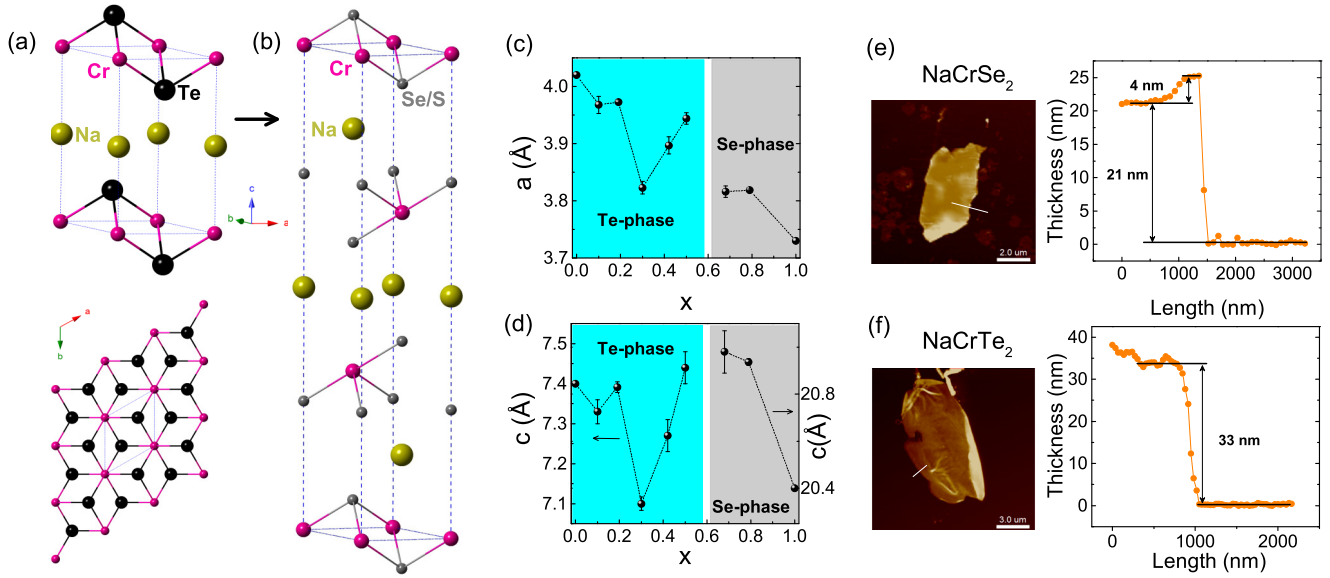
FIG. 1. (a) Crystal structure of NaCrTe$_2$ (top) and top view (bottom) of the CrTe$_2$ layer. The blue dotted lines represent the unit cell. (b) Crystal structure of NaCrSe$_2$ and NaCrS$_2$. (c) and (d) Lattice parameters obtained by fitting single-crystal x-ray diffraction data for NaCr(Te$_{1-x}$Se$_x$)$_2$. (e) and (f) Atomic force microscopy images and height profile step of NaCrSe$_2$ and NaCrTe$_2$ nanoflakes mechanically exfoliated onto a 300 nm SiO$_2$/Si substrate.

show intriguing magnetic and transport properties, including field-induced spin-flip transitions, giant negative magnetoresistance, chemical doping controlled magnetic anisotropy, and conductivity. Our findings suggest the NaCrX$_2$ series contains promising candidates for further investigations in the 2D limit.

II. METHODS

Single crystals of NaCr(Te$_{1-x}$Se$_x$)$_2$ and NaCrS$_2$ were grown by melting stoichiometric elements. High-purity Na, Cr, Te, and Se/S were mixed in the mole ratio 1:1:2(1 − x):2x. These reagents were mixed in alumina crucibles and sealed in an evacuated quartz tube. The assembly was heated up to 1050 °C and maintained at this temperature for 24 h. Then it was slow cooled to 800 °C at a rate of 3 °C/h and annealed at this temperature for 1 day before being furnace cooled to room temperature. In order to make the reaction adequate, before heating to 1050 °C, the assembly stayed for 10 h at temperatures slightly below the melting or boiling point of each reactant. The plane size of the obtained NaCr(Te$_{1-x}$Se$_x$)$_2$ single crystals is up to 6 × 6 mm^2, while the size of NaCrS$_2$ is smaller, typically 1 × 1 mm^2. NaCrTe$_2$ is air sensitive; its shiny surface can be oxidized and discolored after being exposed to the air for a few hours. With Se doping, the crystal become less air sensitive, and it takes about 2 days for NaCrSe$_2$ to degenerate in the air. NaCrS$_2$ is air stable.

We characterized all samples with energy dispersive x-ray spectroscopy (EDS; Oxford X-Max 50). For NaCr(Te$_{1-x}$Se$_x$)$_2$ with $x = 0.1$ and $x = 0.2$, the EDS value is quite close to the nominal value. For $x > 0.3$, the doping concentration may deviate slightly from the nominal value (the estimated error is about 20%). In order to be accurate, all measured samples were carefully checked by EDS. The descriptions in this paper about doping level x all refer to the EDS values.

X-ray diffraction (XRD) values of the samples were collected from a Bruker D8 Advance x-ray diffractometer and a Bruker D8 VENTURE single-crystal diffractometer using Cu $K\alpha$ radiation. Magnetization and electrical transport measurements were carried out using a Quantum Design MPMS3 and PPMS-14T, respectively. The dimensions of exfoliated NaCrTe$_2$ and NaCrSe$_2$ nanoflakes were checked by a Bruker edge dimension atomic force microscope.

III. RESULTS AND DISCUSSION

A. Crystal structure of NaCrX$_2$

As shown in Fig. 1(a) and confirmed by XRD analysis, NaCrX$_2$ crystallizes in a hexagonal structure with a space group of P-3m1 for X=Te and R-3m for X=Se/S, the same as in previous reports [19–21]. The crystal structure of NaCrTe$_2$ can be considered the intercalation of Na atoms between 1T-CrTe$_2$ layers. Na and Cr atoms stack alternately along the c axis in the same site. The Cr atoms form a triangular lattice in the ab plane. When Te was substituted by Se or S, the major change in crystal structure was the interlayer stacking order. In comparison with NaCrTe$_2$, in NaCrSe$_2$ and NaCrS$_2$, both Na and Cr triangular lattice layers are stacked along the c axis with (1/3 1/3) translation in the ab plane. So the c-lattice parameter almost triples. These two different structures are referred to as the "Te phase" and "Se phase," respectively, in the following descriptions.

For NaCr(Te$_{1-x}$Se$_x$)$_2$ $(0 \leqslant x \leqslant 1)$, the lattice parameters were obtained by refining the single-crystal x-ray diffraction data and are plotted in Figs. 1(c) and 1(d). The results show that the samples with $x \leqslant 0.5$ maintain the Te phase, while the samples with $x \geqslant 0.68$ are confirmed to have the Se phase. Therefore, the phase boundary may exist near $x = 0.6$, although it has not been accurately determined. The precession images from the
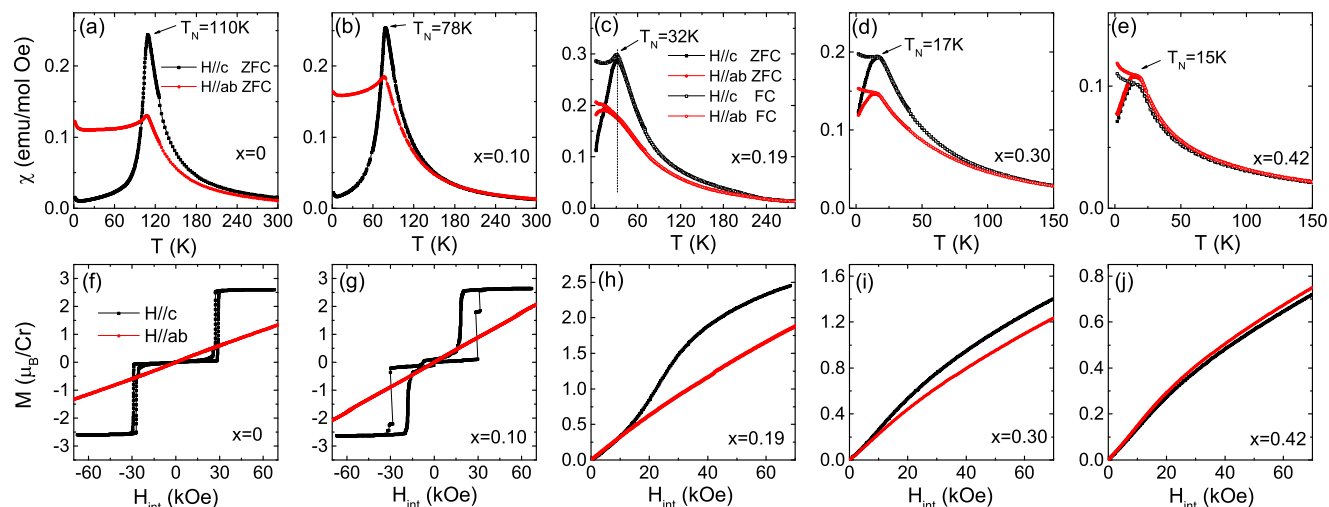
FIG. 2. (a)–(e) The temperature-dependent magnetic susceptibilities measured on $NaCr(Te_{1-x}Se_x)_2$ ($0 \leqslant x \leqslant 0.42$) under magnetic field applied along the *ab* plane or *c* axis. (f)–(j) Magnetization isotherms measured on the same crystals at $T = 2$ K. For $x = 0$ and $x = 0.10$, the hysteresis loops are presented.

single-crystal x-ray diffraction data display streaking features for most doped samples, especially for the heavily doped ones. This indicates that notable stacking disorders and possible phase separations may exist in $NaCr(Te_{1-x}Se_x)_2$ (see Fig. S2 in the Supplemental Material [26]). In the Te-phase zone, both the *a*- and *c*-lattice parameters do not follow a monotonic change with increasing *x*. Compared with $NaCrTe_2$, there is a 7% shrinkage for the *a* axis of $NaCrSe_2$. The *c*-lattice parameter for $NaCrS_2$ is 19.485 Å, which is about 4% lower than that of $NaCrSe_2$.

Previous calculations of the cleavage energies suggested that $NaCrX_2$ can be exfoliated to a thickness of a few layers [18]. We performed mechanical exfoliation of bulk $NaCrX_2$ single crystals using Scotch tape. Nanosheets of $NaCrTe_2$ and $NaCrSe_2$ with thicknesses of 20–30 nm were obtained, as demonstrated by the atomic force microscopy images in Figs. 1(e) and 1(f). Recently, Peng *et al.* demonstrated that isostructural $AgCrS_2$ can be exfoliated into a 1.1 nm nanosheet which consists of one Ag layer sandwiched between two CrS_2 layers [17]. Therefore, this class of materials has promising 2D materials for further investigations. A future investigation on whether $NaCrX_2$ is stable under an exfoliation method similar to that for $AgCrS_2$ could be carried out.

B. Magnetic properties of $NaCr(Te_{1-x}Se_x)_2$

The temperature-dependent magnetic susceptibility $\chi(T)$ and isothermal magnetization $M(H)$ of $NaCr(Te_{1-x}Se_x)_2$ single crystals are shown in Fig. 2. Demagnetization corrections with methods used in our previous publication were applied to the $H \parallel c$ data, and the applied magnetic field H_{app} in the $M(H)$ curve is replaced by the internal field H_{int} [24]. For $NaCrTe_2$, the $\chi(T)$ curve under $H \parallel c$ exhibits a sharp drop down to nearly zero below $T_N = 110$ K, in contrast to the weak cusp and plateaulike feature under $H \parallel ab$. This suggests the development of an *A*-type antiferromagnetic order (ferromagnetic intralayer and antiferromagnetic interlayer

couplings) with the moment aligned along the *c* axis. The Curie-Weiss fit to the high-temperature paramagnetic susceptibility leads to $\mu_{eff}/Cr = 3.8\mu_B$ and $\theta_{CW} = 155$ K. The large positive θ_{CW} value indicates strong intralayer ferromagnetic correlations. The hysteresis loops at 2 K under $H \parallel c$ and $H \parallel ab$ demonstrate the strong perpendicular magnetic anisotropy (PMA) and a spin-flip transition to the ferromagnetic state near $H_{ab} = 30$ kOe. These observations are similar to those in a previous report [20]. The saturation moment for $NaCrTe_2$ is $2.6\mu_B/Cr$, which is a bit lower than the theoretical value of $3.0\mu_B$ for Cr^{3+} in a localized model.

For $x = 0.1$, T_N decreases to 78 K, while the features of *A*-type antiferromagnetic order and perpendicular magnetic anisotropy still persist. The spin-flip transition near 30 kOe also exists but with a much larger hysteresis compared with that of $x = 0$. An important modification of magnetic anisotropy is that the PMA seems to get weakened with Se doping. If we choose the ratio M_c/M_{ab} at $H = 60$ kOe and $T = 2$ K as a criterion, it decreases from 2.3 for $x = 0$ to 1.5 for $x = 0.10$.

With increasing doping concentration *x*, T_N continuously shifts to lower temperature, and the spin-flip transition gradually vanishes as shown in Figs. 2(c), 2(d), and 2(h)–2(j). M_c/M_{ab} at 60 kOe and 2 K also gradually decreases from 1.4 ($x = 0.19$) to 1.2 ($x = 0.30$) and, finally, to 0.95 ($x = 0.42$). This means the magnetic anisotropy gradually evolves from PMA to a slightly preferred in-plane magnetization. On the other hand, for $x \geqslant 0.19$, there is a bifurcation between zero-field-cooling (ZFC) and field-cooling (FC) magnetization below T_N, which implies the emergence of a spin-glass state. In addition, the Curie-Weiss fit to the doped samples reveals similar values of effective moment but lower θ_{CW} values (131–106 K), suggesting slightly weakened ferromagnetic correlations.

The samples with $0 \leqslant x \leqslant 0.42$ discussed above all belong to the Te phase. Our XRD analysis revealed that at least from $x = 0.68$, $NaCr(Te_{1-x}Se_x)_2$ enters the Se phase. Let us first discuss the magnetic properties of $NaCrSe_2$, which
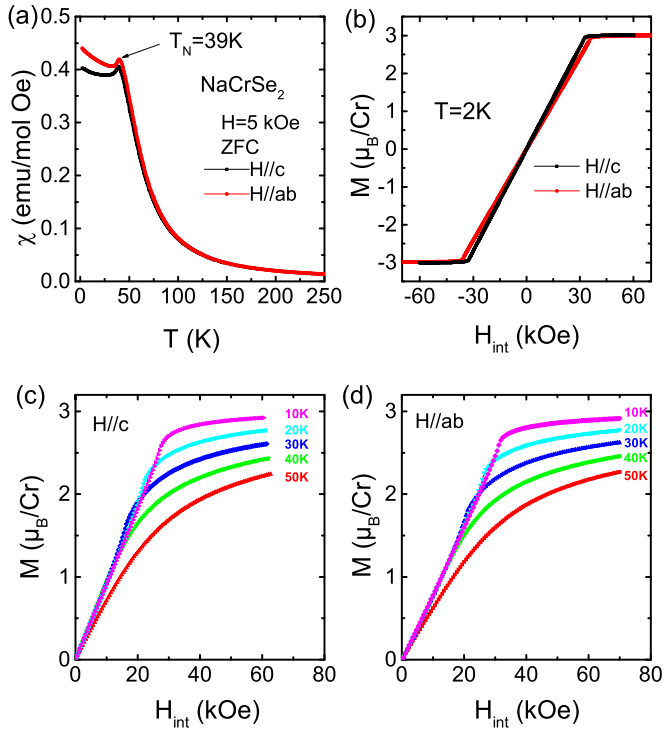
FIG. 3. Anisotropic magnetization data for the NaCrSe$_2$ single crystal: (a) The temperature-dependent magnetic susceptibilities at $H = 5$ kOe. (b) Magnetic hysteresis loops at $T = 2$ K. (c) and (d) Magnetization isotherms measured at selected temperatures under $H \parallel c$ and $H \parallel ab$, respectively.

FIG. 4. (a) The temperature-dependent resistivity of NaCr(Te$_{1-x}$Se$_x$)$_2$ with x=0.1 under zero field. (b) Isothermal magnetoresistance (MR) of x=0.1 under $H \parallel c$.

are shown in Fig. 3. A cusp at $T_N = 39$ K is observed in the $\chi(T)$ curve, indicating an antiferromagnetic transition. On the other hand, fitting the high-temperature paramagnetic data to the Curie-Weiss law yields $\mu_{\mathrm{eff}}/\mathrm{Cr} = 3.8\mu_B$ and $\theta_{\mathrm{CW}} = 108$ K. The positive θ_{CW} temperature indicates ferromagnetic correlations are still strong in each individual layer, while the interlayer coupling is antiferromagnetic, similar to NaCrTe$_2$ and many other 2D layered magnetic materials.

In contrast to the strong anisotropic magnetization under $H \parallel c$ and $H \parallel ab$ for NaCrTe$_2$, the magnetic anisotropy of NaCrSe$_2$ is much smaller. Without applying a demagnetization correction, NaCrSe$_2$ appears to have essentially zero anisotropy. After the correction, a weak PMA could be identified from the $M(H)$ curves at 2 K [Fig. 3(b)]. Under $H \geqslant 30$ kOe for both directions and $T = 2$ K, the magnetization becomes saturated with a saturation moment of $3.0\mu_B/\mathrm{Cr}$, which is larger than that of NaCrTe$_2$ and accurately equals the theoretical value of Cr^{3+} in a localized model. It should be noted that, before reaching a saturated value, the magnetization increases quickly and linearly with increasing field along both directions. This indicates that although the spins of NaCrSe$_2$ are antiferromagnetically aligned at low field, they could be continuously canted along the field direction with increasing field. Figures 3(c) and 3(d) show the $M(H)$ curves at different temperatures. The saturation moment gradually decreases with increasing temperature. At 50 K, which is well above T_N, the $M(H)$ curve still exhibits a nonlinear curvature and a large moment ($\sim 2.2\mu_B/\mathrm{Cr}$) at 60 kOe. In addition, the $M(T)$ curve

also deviates from Curie-Weiss behavior below 200 K, which is actually observed for all NaCrX$_2$ (X=Te,Se,S) samples. These observations suggest that strong magnetic fluctuations or short-range magnetic order may develop well above T_N.

For $x = 0.68$ and $x = 0.79$ with Se phase, the spin-glass behavior is quite similar to that for $x = 0.42$ with Te phase. The related magnetization data are not shown here, but the results are plotted in the phase diagram in Fig. 6 below. Further discussion of the evolution of the anisotropic magnetic properties of NaCr(Te$_{1-x}$Se$_x$)$_2$ is presented in the following section with the phase diagram.

C. Tunable conductivity in NaCr(Te$_{1-x}$Se$_x$)$_2$

Previously, NaCrTe$_2$ was reported to exhibit a metal-insulator-like transition due to the formation of A-type antiferromagnetic ordering [20]. Similarly, the resistivity of the x=0.1 sample has a typical metallic behavior above 130 K [Fig. 4(a)], while a sharp jump appears at T_N=78 K with deceasing temperature, which should result from the localization of charge carriers by long-range antiferromagnetic order. With further deceasing temperature, the resistivity continues to increase with a smaller slope, which might be attributed to the impurity scattering effect from chemical doping. Under magnetic field along the c axis, a giant negative magnetore-
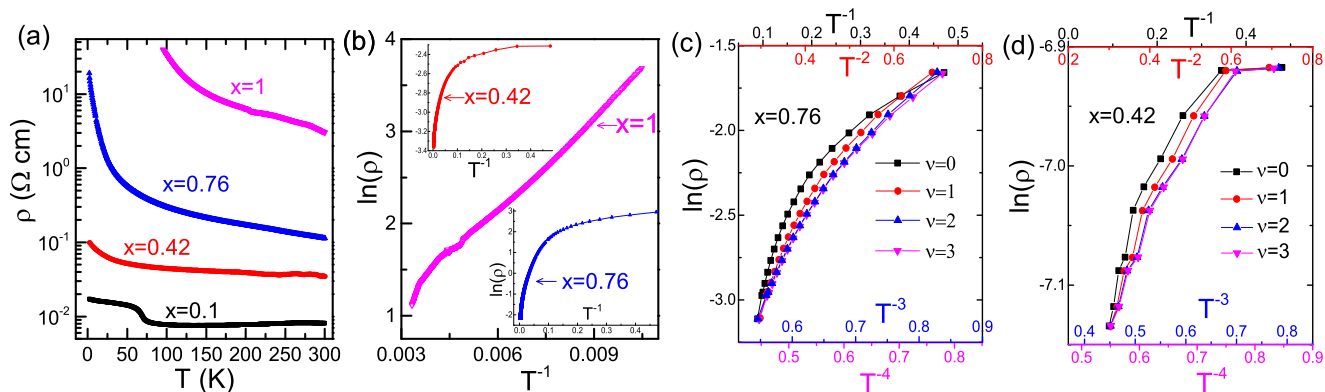
FIG. 5. (a) Temperature-dependent resistivity data for $NaCr(Te_{1-x}Se_x)_2$ ($H = 0$). (b) $Ln\rho$ versus T^{-1} plot of $x=1$ for all measured temperatures. The inset shows the same plots for $x=0.42$ and $x=0.76$. (c) and (d) Low-temperature $\ln\rho$ versus $T^{-1/(\nu+1)}$ plots of $x=0.76$ and $x=0.42$, respectively. ν is the parameter from the VRH formula.

sistance appears with a maximal value up to 48% at 5 K and 70 kOe. This behavior is directly associated with the field-induced spin-flip transition and due to the reduced spin scattering of the electrons in the ferromagnetic state compared with that in the antiferromagnetic states.

In a comparison with the previously reported resistivity of $NaCrTe_2$ [20], we noticed that the value for $x=0.1$ approximately increases by an order of magnitude. As shown in Fig. 5(a), intriguingly, with further increasing Se-doping concentration x, the temperature-dependent resistivity of $NaCr(Te_{1-x}Se_x)_2$ becomes fully semiconductinglike, and the absolute value of resistivity continuously increases by several orders. For $NaCrSe_2$ with $x=1$, the resistivity is about ~ 10 Ω cmm and the data below 95 K cannot be obtained due to the upper limit of physical property measurement system measurement. Thus, a Se-doping-induced metal-insulator transition is observed for $NaCr(Te_{1-x}Se_x)_2$.

Density functional theory calculations have shown that both $NaCrTe_2$ and $NaCrSe_2$ are semiconductors; their band gaps are 0.59 and 0.77 eV, respectively [18]. In order to check whether the doping controlled conductivity is due to the gradual increasing of the band gap, we have tried to fit the resistivity data using the thermal activation model as described by $\rho=\rho_0\exp(E_a/2k_BT)$, where E_a is the energy gap and k_B is the Boltzmann constant. Therefore, a fine fitting result using this formula can be obtained only when $\ln\rho$ and T^{-1} follow a linear relationship. However, as shown in Fig. 5(b), there are not well-defined linear relations between $\ln\rho$ and T^{-1} for all samples, especially for $x=0.42$ and $x=0.76$.

For chemical-doped samples, the doping-induced strong disorder potential might trap itinerant electrons and lead to a metal-insulator transition, which is the famous Anderson localization [27]. For an Anderson insulator at low temperatures, there are electronic states trapped in the vicinity of the Fermi surface, and the hopping transport of localized electrons would be described by the variable range hopping (VRH) model $\rho=\rho_0\exp(T_0/T)^{1/(\nu+1)}$ [28]. In this formula, $\nu=0$ denotes the traditional insulator with a band gap (the same as the thermal activation model described above). $\nu=1$, 2, and 3 correspond to one-, two-, and three-dimensional materials with Anderson localization, respectively. Figures 5(c) and 5(d) present the $\ln\rho$ versus $T^{-1/(\nu+1)}$ plots for $x=0.42$

and 0.76 from 2 to 10 K. Although a perfect straight line is not observed, the formula using $\nu=2$ or $\nu=3$ clearly gives much better fitting results compared with that using $\nu=0$, especially for $x=0.76$. Our results indicate that the significant enhancement of resistivity in $NaCr(Te_{1-x}Se_x)_2$ may partially originate from the Anderson localization. In addition, tuning the band gap by Se doping would also be possible. The electronic transport properties of $NaCr(Te_{1-x}Se_x)_2$ may contain contributions from these two aspects.

D. Discussion of the phase diagram of $NaCr(Te_{1-x}Se_x)_2$

The T-x phase diagram of $NaCr(Te_{1-x}Se_x)_2$ is presented in Fig. 6, which summarizes the major experimental results above. Three features of this phase diagram should be mentioned. First, considering either Se-doped $NaCrTe_2$ or Te-doped $NaCrSe_2$, the antiferromagnetic transition temperature gradually decreases, and the system enters a spin-glass state with increasing doping concentration. Second, the magnetic anisotropy can be effectively tuned by chemical doping
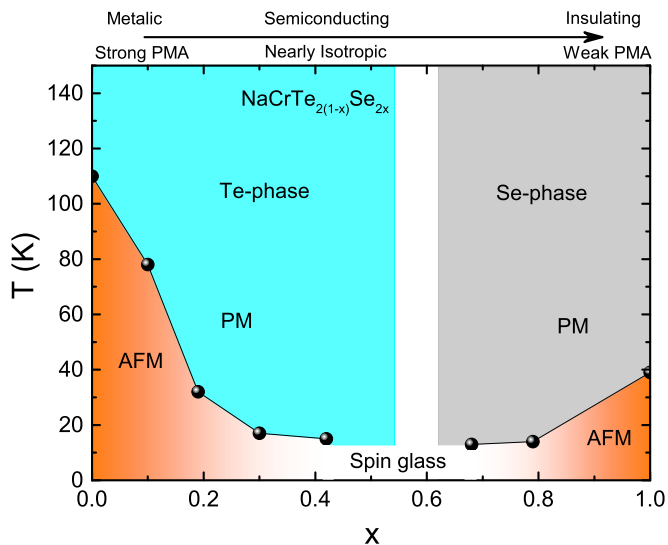
FIG. 6. Temperature versus doping phase diagram for $NaCr(Te_{1-x}Se_x)_2$ ($0 \leqslant x \leqslant 1$).
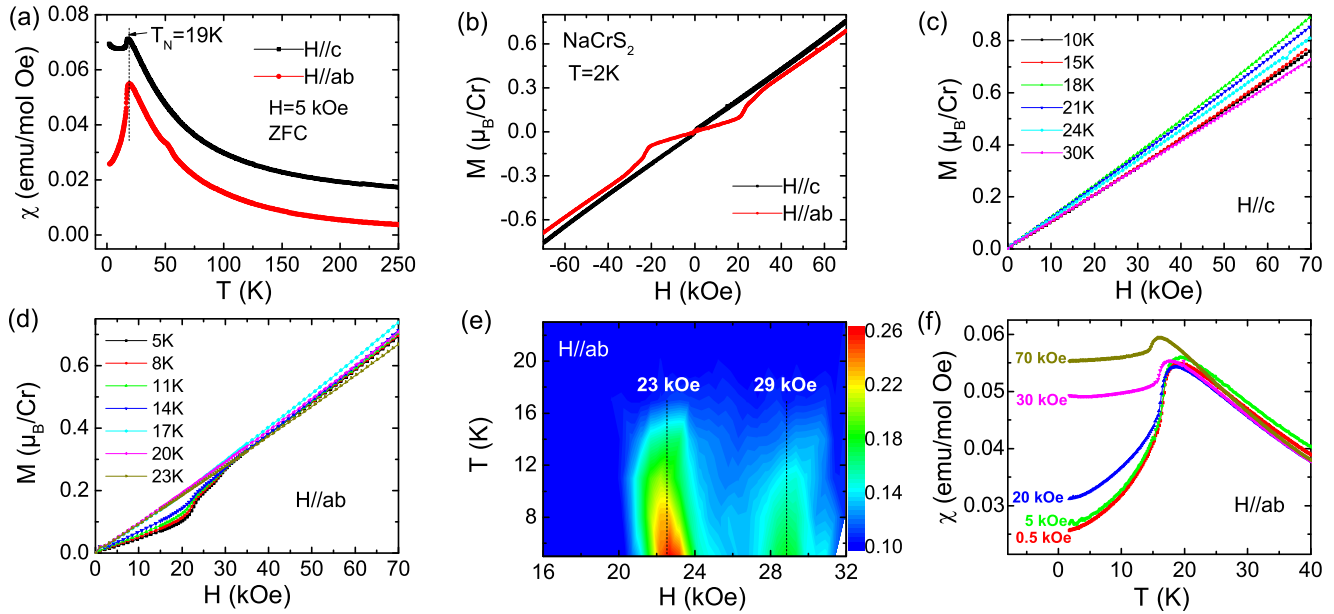
FIG. 7. Anisotropic magnetization data for the $NaCrS_2$ single crystal: (a) The temperature-dependent magnetic susceptibilities at $H = 5$ kOe. (b) Magnetic hysteresis loops at $T = 2$ K. (c) and (d) Magnetization isotherms measured at selected temperatures under $H \parallel c$ and $H \parallel ab$, respectively. (e) Contour plot of dM/dH as a function of temperature and field along $H \parallel ab$. (f) The temperature-dependent magnetic susceptibilities under different applied fields near the antiferromagnetic transition.

in this system. $NaCrTe_2$ possesses a strong PMA, and it continuously gets weakened and evolves into a nearly isotropic magnetic behavior at $x = 0.42$ while retaining the Te phase. For $NaCrSe_2$ at the other end, a weak PMA is identified. Third, a systematic change in the conductivity of $NaCr(Te_{1-x}Se_x)_2$ occurs on increasing x, from bad metallic behavior in $NaCrTe_2$ to semiconducting or insulating behavior in $NaCrSe_2$.

The doping-induced disorder effect and stacking faults should be responsible for the emergence of the spin-glass state [29]. They also may play important roles in tuning the magnetic anisotropy in $NaCr(Te_{1-x}Se_x)_2$. In previous investigations of materials for high-density magnetic recording media, chemical disorder was shown to have an important influence on the magnetocrystalline anisotropy energy (MAE) [30–32]. It may either drastically reduce the MAE or tune the MAE to a maximum value [30–32]. For vdW materials, recent studies revealed that $Ni_{1-x}Fe_xPS_3$ and $Fe_{5(1-x)}Co_{5x}GeTe_2$ enable chemical tuning of easy-plane and easy-axis anisotropies [24,25,33]. Magnetic anisotropy is a key property of 2D magnets, which is required for counteracting thermal fluctuations. There have been reports of pressure control of magnetic anisotropy in $CrGeTe_6$ [34] and tensile-strain-tunable magnetic anisotropy in monolayer CrX_3 (X = Cl, Br, I) [35]. Our study provides a different example of chemical disorder or stacking fault controlled magnetic anisotropy in the 2D magnetic material $NaCr(Te_{1-x}Se_x)_2$.

In addition, one should notice that the magnetic anisotropy also makes a big difference between $NaCrTe_2$ and $NaCrSe_2$; neither seems to have any evident chemical disorder. A possibility is that, for $NaCrSe_2$ with a relatively much lighter Se element, the spin-orbit coupling effect may become weak and results in a weak PMA [36]. As we mentioned above, the saturation moment of $NaCrSe_2$ agrees well with the expectation of the Cr^{3+} spin $S = 3/2$ model without orbital moment, while

that of $NaCrTe_2$ has a notably smaller value which might be due to enhanced spin-orbital coupling.

The tuning of conductivity by chemical doping in 2D magnetic materials has rarely been reported. This effect found in $NaCr(Te_{1-x}Se_x)_2$, possibly due to Anderson localization and the change in band structure, may have important applications in designing novel spintronic devices. Particularly, the chemical doping in $NaCr(Te_{1-x}Se_x)_2$ could simultaneously tune both the conductivity and magnetic anisotropy.

E. Field-induced metamagnetic transitions in $NaCrS_2$

For the magnetic properties of $NaCrS_2$, as far as we know, there have not been any investigations of the single crystals. We present anisotropic magnetization data for $NaCrS_2$ single crystals in Fig. 7. The different temperature-dependent features of χ_{ab} and χ_c below $T_N = 19$ K indicate the ordered magnetic moment should be confined within the ab plane [Fig. 7(a)]. Figure 7(b) present the magnetic hysteresis loops at 2 K. Under magnetic field applied along the hard axis ($H \parallel c$), a linear relationship between magnetization and field is observed. But for field applied along the easy ab plane, a sudden magnetization jump is revealed at around 25 kOe, suggesting the occurrence of a field-induced metamagnetic transition. From the magnetization isotherms at higher temperatures [Figs. 7(c) and 7(d)], the linear behavior persists for $H \parallel c$, and the magnetization jump gradually weakens with increasing temperature for $H \parallel ab$. The contour plot of dM_{ab}/dH in Fig. 7(e) reveals that there are actually two metamagnetic transitions which appear at $H = 23$ kOe and $H = 29$ kOe. These two transitions gradually disappear near T_N. The transition at lower field slightly softens with increasing temperature, similar to that for a conventional spin-flop transition.

Early neutron diffraction results for $NaCrS_2$ powders have determined its magnetic structure is an in-plane helical one [21]. The spins of Cr have antiferromagnetic coupling along the c axis, while in the ab plane they are aligned in a helimagnetic order with rotating angle $\phi = 33°$ in adjacent (110) planes [21]. This ground state magnetic structure is consistent with the anisotropic magnetic behavior of our single-crystal sample. It is interesting to point out that the Curie-Weiss fit still gives positive θ_{CW} values (18 K for $H \parallel ab$ and 31 K for $H \parallel c$), which suggests the ferromagnetic correlations still exist. In addition, we noticed that the paramagnetic susceptibility and corresponding fitted θ_{CW} values have large anisotropy. Whether this really indicates the anisotropy of the exchange interactions requires further research to clarify, as this kind of difference can arise solely from the single-ion anisotropy even without exchange interaction as in previous theoretical research [37].

Furthermore, the observed field-induced metamagnetic transitions should have significant influence on this complex helimagnetic order. First, the magnetic order under field above 30 kOe should also be antiferromagneticlike. This is supported by the cusplike feature in the χ_{ab}-T curve at T_N, as shown in Fig. 7(f). The antiferromagnetic transition seems to be quite robust under field. T_N has only a slight shift to 16 K under $H = 70$ kOe. In addition, the $M(H)$ curve follows a linear relationship up to 70 kOe with a small moment ($\sim 0.7 \mu_B$/Cr) under this field. Second, for $H_{ab} \leqslant 20$ kOe the magnetic susceptibilities show a sharp drop below T_N. In contrast, for $H_{ab} = 30$ and 70 kOe, the magnetic susceptibilities exhibit a plateau below T_N, which is a typical feature of canted antiferromagnetic magnetic order. Therefore, new types of antiferromagnetic order are expected under in-plane magnetic field, which would be an interesting topic for further investigations using neutron scattering.

IV. CONCLUSIONS

In summary, the physical properties of $NaCrX_2$ (X=Te,Se,S) were investigated in single-crystal form. For $NaCr(Te_{1-x}Se_x)_2$, a field-induced spin-flip transition together with a giant negative magnetoresistance were observed at $x \leqslant 0.1$. At higher doping levels, a spin-glass state emerges. The most prominent feature is that both the magnetic anisotropy and the conductivity can be effectively tuned by x. For $NaCrS_2$, two magnetic field induced metamagnetic transitions were identified. We further demonstrated that these crystals can be mechanically exfoliated into nanoflakes. These properties make $NaCrX_2$ a promising material playground for further investigations of 2D magnetism and for designing novel magnetoelectronic devices. Furthermore, our samples also provide a route to vdW layered CrX_2 through deintercalation.

[1] K. S. Burch, D. Mandrus, and J.-G. Park, Nature (London) **563**, 47 (2018).

[2] H. Li, S. Ruan, and Y.-J. Zeng, Adv. Mater. **31**, 1900065 (2019).

[3] D. L. Cortie, G. L. Causer, K. C. Rule, H. Fritzsche, W. Kreuzpaintner, and F. Klose, Adv. Funct. Mater. **30**, 1901414 (2020).

[4] Y. Deng, Y. Yu, Y. Song, J. Zhang, N. Z. Wang, Z. Sun, Y. Yi, Y. Z. Wu, S. Wu, J. Zhu, J. Wang, X. H. Chen, and Y. Zhang, Nature (London) **563**, 94 (2018).

[5] Z. Fei, B. Huang, P. Malinowski, W. Wang, T. Song, J. Sanchez, W. Yao, D. Xiao, X. Zhu, A. F. May, W. Wu, D. H. Cobden, J.-H. Chu, and X. Xu, Nat. Mater. **17**, 778 (2018).

[6] B. Huang, G. Clark, E. Navarromoratalla, D. R. Klein, R. Cheng, K. L. Seyler, D. Zhong, E. Schmidgall, M. A. Mcguire, and D. H. Cobden, Nature (London) **546**, 270 (2017).

[7] C. Gong, L. Li, Z. Li, H. Ji, A. Stern, Y. Xia, T. Cao, W. Bao, C. Wang, and Y. Wang, Nature (London) **546**, 265 (2017).

[8] J.-U. Lee, S. Lee, J. H. Ryoo, S. Kang, T. Y. Kim, P. Kim, C.-H. Park, J.-G. Park, and H. Cheong, Nano Lett. **16**, 7433 (2016).

[9] X. Wang, K. Du, Y. Y. F. Liu, P. Hu, J. Zhang, Q. Zhang, M. H. S. Owen, X. Lu, C. K. Gan, P. Sengupta, C. Kloc, and Q. Xiong, 2D Mater. **3**, 031009 (2016).

[10] D. C. Freitas, R. Weht, A. Sulpice, G. Remenyi, P. Strobel, F. Gay, J. Marcus, and M. Núñez-Regueiro, J. Phys.: Condens. Matter **27**, 176002 (2015).

[11] X. Sun *et al.*, Nano Res. **13**, 3358 (2020).

[12] X. Zhang, Q. Lu, W. Liu, W. Niu, J. Sun, J. Cook, M. Vaninger, P. F. Miceli, D. J. Singh, S.-W. Lian, T.-R. Chang, X. He, J. Du, L. He, R. Zhang, G. Bian, and Y. Xu, Nat. Commun. **12**, 2492 (2021).

[13] L. Meng, Z. Zhou, M. Xu, S. Yang, K. Si, L. Liu, X. Wang, H. Jiang, B. Li, P. Qin, P. Zhang, J. Wang, Z. Liu, P. Tang, Y. Ye, W. Zhou, L. Bao, H.-J. Gao, and Y. Gong, Nat. Commun. **12**, 809 (2021).

[14] F. Fabre, A. Finco, A. Purbawati, A. Hadj-Azzem, N. Rougemaille, J. Coraux, I. Philip, and V. Jacques, Phys. Rev. Mater. **5**, 034008 (2021).

[15] J.-J. Xian, C. Wang, J.-H. Nie, R. Li, M. Han, J. Lin, W.-H. Zhang, Z.-Y. Liu, Z.-M. Zhang, M.-P. Miao, Y. Yi, S. Wu, X. Chen, J. Han, Z. Xia, W. Ji, and Y.-S. Fu, Nat. Commun. **13**, 257 (2022).

[16] M. Huang, Z. Ma, S. Wang, S. Li, M. Li, J. Xiang, P. Liu, G. Hu, Z. Zhang, Z. Sun, Y. Lu, Z. Sheng, G. Chen, Y.-L. Chueh, S. A. Yang, and B. Xiang, 2D Mater. **8**, 031003 (2021).

[17] J. Peng, Y. Liu, H. Lv, Y. Li, Y. Lin, Y. Su, J. Wu, H. Liu, Y. Guo, Z. Zhuo, X. Wu, C. Wu, and Y. Xie, Nat. Chem. **13**, 1235 (2021).

[18] W. Xu, S. Ali, Y. Jin, X. Wu, and H. Xu, ACS Appl. Electron. Mater. **2**, 3853 (2020).

[19] S. Kobayashi, H. Ueda, C. Michioka, and K. Yoshimura, Inorg. Chem. **55**, 7407 (2016).

[20] J. Wang, J. Deng, X. Liang, G. Gao, T. Ying, S. Tian, H. Lei, Y. Song, X. Chen, J.-G. Guo, and X. Chen, Phys. Rev. Mater. **5**, L091401 (2021).

[21] F. Engelsman, G. Wiegers, F. Jellinek, and B. Van Laar, J. Solid State Chem. **6**, 574 (1973).

[22] C.-K. Tian, C. Wang, W. Ji, J.-C. Wang, T.-L. Xia, L. Wang, J.-J. Liu, H.-X. Zhang, and P. Cheng, Phys. Rev. B **99**, 184428 (2019).

[23] J. Sheng, X. Li, C. Tian, J. Song, X. Li, G. Sun, T. Xia, J. Wang, J. Liu, D. Xu, H. Zhang, X. Tong, W. Luo, L. Wu, W. Bao, and P. Cheng, Phys. Rev. B **101**, 174516 (2020).

[24] C. Tian, F. Pan, S. Xu, K. Ai, T. Xia, and P. Cheng, Appl. Phys. Lett. **116**, 202402 (2020).

[25] S. Lee, J. Park, Y. Choi, K. Raju, W.-T. Chen, R. Sankar, and K.-Y. Choi, Phys. Rev. B **104**, 174412 (2021).

[26] See Supplemental Material at http://link.aps.org/supplemental/ 10.1103/PhysRevMaterials.6.094013 for details about the structural and composition analysis of $NaCr(Te_{1-x}Se_x)_2$ through single-crystal x-ray diffraction and EDS.

[27] P. W. Anderson, Phys. Rev. **109**, 1492 (1958).

[28] T. Ying, Y. Gu, X. Chen, X. Wang, S. Jin, L. Zhao, W. Zhang, and X. Chen, Sci. Adv. **2**, e1501283 (2016).

[29] K. Binder and A. P. Young, Rev. Mod. Phys. **58**, 801 (1986).

[30] C. J. Aas, L. Szunyogh, J. S. Chen, and R. W. Chantrell, Appl. Phys. Lett. **99**, 132501 (2011).

[31] M. Si, A. Izardar, and C. Ederer, Phys. Rev. Res. **4**, 033161 (2022).

[32] C. Neise, S. Schonecker, M. Richter, K. Koepernik, and H. Eschrig, Phys. Status Solidi B **248**, 2398 (2011).

[33] A. F. May, M.-H. Du, V. R. Cooper, and M. A. McGuire, Phys. Rev. Mater. **4**, 074008 (2020).

[34] T. Sakurai, B. Rubrecht, L. T. Corredor, R. Takehara, M. Yasutani, J. Zeisner, A. Alfonsov, S. Selter, S. Aswartham, A. U. B. Wolter, B. Büchner, H. Ohta, and V. Kataev, Phys. Rev. B **103**, 024404 (2021).

[35] L. Webster and J.-A. Yan, Phys. Rev. B **98**, 144411 (2018).

[36] F. Xue, Y. Hou, Z. Wang, and R. Wu, Phys. Rev. B **100**, 224429 (2019).

[37] D. C. Johnston, Phys. Rev. B **95**, 094421 (2017).